Low-Temperature Sintering of Cu/Functionalized Multiwalled Carbon Nanotubes Composite Paste for Power Electronic Packaging

Lingmei Wu, Jing Qian, Fusheng Zhang, Jiabing Yu, Zeping Wang, Haojie Guo, and Xianping Chen, *Senior Member, IEEE*

***Abstract*—Sintered Cu is considered as the most promising strategy in die-attachment, since its capacities of low-temperature bonding and high-temperature working. Many studies have reported the excellent properties of sintered Cu, but there is still some room for improvement. Here, strong Cu–Cu joints and insulated-gate bipolar transistor (IGBT) devices are achieved by sintering Cu paste and three composite pastes, and the mechanical, electrical, and microstructure properties of joints are investigated. The shear strength of pure Cu bonded joint is 23.4 MPa, which is improved to 26.64 MPa by introducing 0.6 wt% N-doped multi-walled carbon nanotubes (N-doped MWCNTs) into Cu paste. Excellent electrical properties are achieved as the resistivities of sintered Cu/N-doped MWCNTs layer and Cu/carboxylated WMCNTs are 2.252 and 2.551 $\mu\Omega$·cm, respectively, which are lower than the sintered pure Cu layer (3.473 $\mu\Omega$·cm). In addition, the functionalized MWCNTs are found exerted positive effects on the joint reliability. The enhancements on the joint qualities are attributed to that the functionalized MWCNTs improve the affinity of the Cu and CNTs and increase the density of bonding layer. This article provides an effective way to improve the sintered Cu joints sintering qualities, which is suitable for the attachment of next-generation devices and substrates.**

Manuscript received February 20, 2021; revised May 8, 2021 and July 6, 2021; accepted August 2, 2021. Date of publication August 10, 2021; date of current version October 15, 2021. This work was supported in part by the National Natural Science Foundation of China under Grant 62071073, in part by the National Key Research and Development Program under Grant 2018YFB2100100, in part by the Fundamental Research Funds for Central Universities under Grant 2019CDJGFGD007, in part by the Key Science and Technology Program of Chongqing under Grant CSTC2017SHMS-ZDYFX0028, in part by the Technology Innovation and Application Project of Chongqing under Grant cstc2018jszx-cyzdX0111, in part by the China Postdoctoral Science Foundation under Grant 2019M663433, and in part by the Guangxi Key Laboratory of Manufacturing Systems and Advanced Manufacturing Technology under Grant 19-050-44-002K. Recommended for publication by Associate Editor K. Ngo. *(Corresponding author: Xianping Chen.)*

Lingmei Wu, Jing Qian, Fusheng Zhang, and Xianping Chen are with the School of Electrical Engineering and State Key Laboratory of Power Transmission Equipment and System Security and New Technology, Chongqing University, Chongqing 400044, China (e-mail: 201911021034@cqu.edu.cn; jingleqian@outlook.com; 201911021042@cqu.edu.cn; xianpingchen@cqu.edu.cn).

Jiabing Yu, Zeping Wang, and Haojie Guo are with the College of Optoelectronic Engineering and Key Laboratory of Optoelectronic Technology and Systems Education Ministry of China, Chongqing University, Chongqing 400044, China (e-mail: yujiab@cqu.edu.cn; zepingwang@cqu.edu.cn; 201908131074@cqu.edu.cn).

This article has supplementary material provided by the authors and color versions of one or more figures available at https://doi.org/10.1109/TPEL.2021.3103563.

Digital Object Identifier 10.1109/TPEL.2021.3103563

***Index Terms*—Cu/functionalized multiwalled carbon nanotubes (MWCNTs) composite paste, Cu–Cu joints, die attach, sintered Cu.**

I. Introduction

THE third-generation semiconductor materials represented by Silicon Carbide (SiC) and Gallium Nitride (GaN), usually known as wide bandgap semiconductor (WBG) materials, have attracted widespread attention and got rapid development [1]–[3]. The WBG power devices are suitable for high temperature, high frequency, and other such harsh environments [4]. In practical application, whether WBG power devices can work reliably and efficiently in harsh environments depends not only on the devices themselves, but also on the properties of packaging materials, especially the die attachment materials. The traditional packaging materials, such as Sn-based solders, and other alloy solders are not applicable due to their low melting points and inadequate electrical and thermal conductivity [5]–[7]. Thus, it is important to develop an environmentally friendly bonding material, which can not only support working in high temperature, but also possess excellent electrical and thermal properties.

Recently, sintered Ag and Cu are proposed as alternative packaging technologies for WBG devices, thanks to their excellent characteristics [8]–[12]. But the widespread adoption of sintered-Ag is limited by the high price and electrochemical migration [13]. Compared to Ag, sintered Cu overcomes the drawbacks and shows equal mechanical, electrical, and thermal properties. Thus, the bonding technology of sintering of Cu NPs has received the increased attention [14], [15]. However, the bonding technology has been plagued by the oxidation of Cu. The copper oxidation not only disturbs the sintering behavior of Cu NPs and further damages the properties of sintered Cu, but also extremely deteriorates the reliability of the joints. To protect Cu from oxidizing during preparation and improve the sintering qualities, a series of attempts including surface passivation (coating the organic protective layer) [16], [17], sintering in reductive/insert atmosphere [18]–[20], and forming a mental core–shell structure [21] have been made. Thereinto, sintering in an atmosphere that contained reductive and inert gas is regarded as an effective, economical, and most widely used method. However, the amount of reducing gas required has not been determined. The other approaches have their own

drawbacks, including high sintering temperature, complicated synthesis process, and inferior electrical conductivity. As for the inadequate long-term reliability, it has been reported that improving the paste packing density and reducing the porosity of the bonding layer are effective in building high reliable sintered Cu joints [22], [23]. The research on the reliability of sintered Cu NPs is very limited. Ishizaki *et al.* [24], [25] tested the reliability of sintered Cu NPs bonded joints by power cycle and thermal cycle, and found that the joints sintered at 350 °C can endure 3000 power cycles of 65/250 °C and 1000 thermal cycles of −40/ 200 °C . Usui *et al.* [22] reported that the thermal aging (250 °C for 100 h) decreased the sintered Cu NPs joint strength greatly and the high temperature stability of joint can be improved by adding eutectic Bi–Sn powder. However, this method may sacrifice part of the excellent electrothermal properties of sintered Cu. A solution that concurrently guarantee the mechanical, electrical properties, and long-term reliability of sintered-Cu remains elusive.

Carbon nanotubes (CNTs), which has exceptional thermal conductivity (3500 $W{\cdot}m^{-1}K^{-1}$), electrical conductivity ($2 \times 107\ S{\cdot}m^{-1}$) and cheap price, are considered as very promising materials for electrical conductors [26]–[28]. So far, some studies have verified that the addition of CNTs is able to enhance the mechanical, electrical, and thermal characters of Cu NPs [28], [29]. For instance, Hak-Sung Kim *et al.* [30] achieved high conductive Cu/CNTs composite films (7.86 $\mu\Omega{\cdot}$cm). However, due to the poor affinity of Cu and the CNTs, it is difficult to obtain a strong adhesive strength at the interfaces. Additionally, the CNTs are easily to agglomerate in the copper matrix, which could lead to a performance degradation of Cu/CNTs composites [31], [32]. Fortunately, recent studies predicted that the functional groups of CNTs can enhance the bonding strength of Cu and CNTs and further improve the mechanical and electrical properties by the simulation calculation [33]. It is reported by Park *et al.* [34] that the oxygen-containing functional groups, especially the carboxyl groups enhance the interfacial bonding between Cu and CNTs. Kim *et al.* [35] demonstrated experimentally that oxygen atoms not only improve the adhesion and load transfer between Cu and CNTs, but also better the dispersion of CNTs in metal matrix.

To date, few research works attempt to improve the qualities of sintered Cu NPs by mixing functionalized MWCNTs with Cu paste. In this article, based on previous research works, we introduce the functionalized MWCNTs including N-doped MWCNTs and carboxylated MWCNTs into the Cu paste to improve the qualities of sintered Cu joint. For comparison, the MWCNTs are also mixed with Cu paste to prepare the Cu/MWCNTs composite paste. Large-area Cu–Cu joints composed of Si chips coated by Ti/Ni/Cu layers and direct bond copper (DBC) substrates are fabricated by pure Cu paste and three kinds Cu/CNTs composite pastes. The insulated-gate bipolar transistor (IGBT) devices are attached to the DBC substrates by sintering the four types paste. We determine the presintering temperature and sintering atmosphere at first, and explore the effect of three CNTs weight fraction with regard to enhance the joints strength. It is found that the shear strength of sintered Cu joint can be improved from 23.83 to 26.64 MPa by mixing 0.6 wt% N-doped MWCNTs with Cu paste, which means

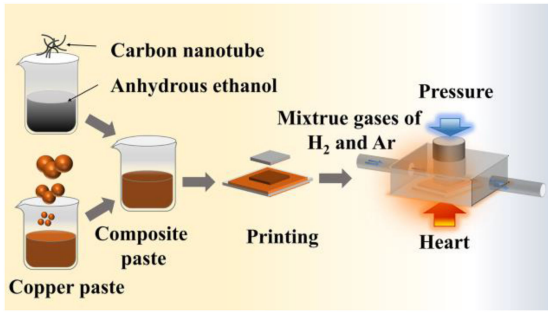

Fig. 1. Schematic depicting the synthesis of Cu paste and Cu/CNTs composite paste, and the joints bonding process.

that a highly strength large-area joint has been achieved. In addition, the resistivity of the sintered Cu/N-doped MWCNTs and Cu/carboxylated MWCNTs films, and the static output *I–V* curves of IGBT are measured to verify the superiority of sintered Cu/functionalized MWCNTs. We found also that the two types functionalized MWCNTs exerted a positive on the joint reliability. The microstructure of sintered layer is analyzed by SEM and TEM. Our experiments confirm the theoretical predictions putted by Milowska *et al*. [33] and achieved high performance Cu–Cu joints. Therefore, we believe that the Cu/functionalized MWCNTs composite paste is a superior die-attach material for high-temperature power devices.

II. Experimental Procedure

A. Preparation of Cu Particles/CNTs Composite Paste

The Cu paste used in this article was prepared at first by mixing multiscale copper particles and several organic solvents with mass percents of 88 and 12 wt%, respectively. The multiscale Cu particles are composed of spherical NPs (20–60 nm), submicro-particles (0.2–0.6 μm), and micro-particles (1–2 μm). It has reported that the original pack density can be improved by mixing Cu microparticles and NPs [23], [36]. The fabrication process is shown in Fig. 1. In this article, three kinds CNTs, including MWCNTs, N-doped MWCNTs, and carboxylated MWCNTs are involved, which were obtained from Xfnano, Inc (NanJing, China, www.Xfnano.com). The outer diameter and length of the three kinds CNTs are ranging from 20 to 80 nm and 10 to 30 μm, respectively. There are three types N dopants (pyridinic, pyrrolic, and quaternary nitrogen groups) with a percent of 5.01 at% present in the N-doped MWCNTs, which can be confirmed by XPS analysis and the results are shown in Fig. S2. The oxygen-bearing groups in carboxylated MWCNTs including carboxyl (-COOH), hydroxy (-OH), and oxygen (-O) groups, and the more details about CNTs we used are shown in the Supplementary Materials. The content of carboxyl group is about 0.7 wt%. To improve the dispersion, the CNTs were mixed with anhydrous ethanol with a mass ratio of 100:1 and then treated by ultrasound for 1 h. The treated mixture of CNTs and ethanol was evenly mixed with Cu paste to prepare composite paste, which was finally printed on the substrate. To investigate the effect of the percent of the CNTs on the qualities of the large-area Cu–Cu joints, the weight fraction of CNTs in the copper paste is varying from 0.0 to 1.2 wt%.

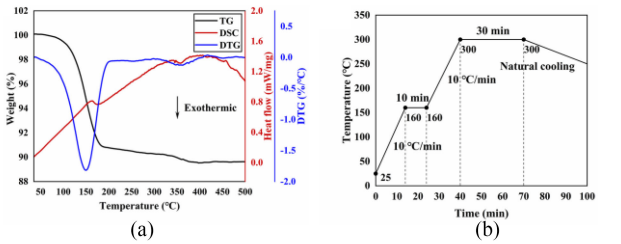

Fig. 2. (a) TG–DSC curves. (b) Sintering temperature curves.

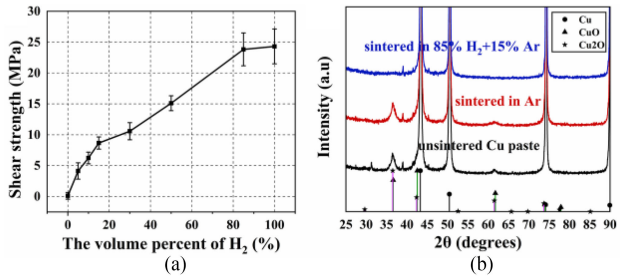

Fig. 3. (a) Shear strength of joint Cu paste bonded in different atmosphere. (b) XRD pattern of the Cu paste.

B. Preparation of Large-Area Cu–Cu Joints and IGBT Devices

To remove the Cu oxidation and create mechanical interlocks [15], the DBC substrates were treated by 100 grits sandpapers at first, then cleaned in ultrasonic for 10 min and washed by anhydrous ethanol at last. The Si chips were coated by Ti/Ni/Cu metallization. The dimensions of the chips and DBC substrates are 10 mm × 10 mm × 0.80 mm and 20 mm × 20 mm × 1.20 mm, respectively. A layer thickness of 80 μm was printed on the Cu substrates to build Cu–Cu joints to be sintered. Eight Si based IGBT (3300 V/50 A) devices with size of 13.5 mm × 13.5 mm × 0.58 mm were prepared to attached on the same DBC substrates. More details about the IGBT chips will be given in the Supplementary Materials. Then, the Al wires with a diameter of 0.2 mm are bonded to the three electrodes of the IGBT devices by ultrasonic bonding (PowerFusion TL2). The main three factors that affect the wire-bond quality are ultrasonic power, bond time, and bond force, which are set as 38.0–45.0 mW, 70–80 ms, and 380–400 gf, respectively. The prepared IGBT devices are shown in Fig. S5. The sandwich-like samples will be sintered in 300 °C for 30 min with an assist pressure of 5 MPa. Before sintering, differential scanning calorimetry (DSC) and thermogravimetric analysis (TGA) were tested to obtain optimal presintering temperature. To investigate the demand of H_2, the sintering atmosphere mixed by Ar and H_2 gas, in which, the volume percentages of H_2 change from 0% to 100%.

C. Determine of the Presintering Temperature and Atmosphere

To ensure the complete removal of organic solvents and improve the sintering qualities, a presintering process is needed for large-area Cu–Cu joints. DSC and TGA curves are synchronously tested by NETZSCH STA 449 F3/F5 TGA in N_2 atmosphere to evaluate the thermal behavior of Cu paste and help to determine the presintering temperature. The temperature increased from 30 to 500 °C with a heating rate of 10 °C/min. Fig. 2(a) presents the TG–DSC curves of the Cu paste, as shown in the TG curve (black), the weight of the Cu paste decreased obviously at about 150 °C. A weight loss about 9.29% has been measured, which is mainly caused by the evaporation of the organic solvents. The DSC curve reveals an endothermic peak around 150 °C. This is due to the absorption of heat by the evaporation of organic solvents. In addition, the TGA curve indicates that the weight change rate of Cu paste is the fastest at 150 °C. For these reasons, a presintering process with a temperature of 160 °C was designed to promote the effective removal of organic solvents. The sintering temperature curve was shown in Fig. 2(b), the sintering temperature is 300 °C and the heating rate is 10 °C /min.

To investigate the optimal volume fraction of H_2, large-area Cu–Cu joints are bonded in a mixture atmosphere of H_2 and Ar with a total flow of 100 mL/min. The shear strength, tested by microcomputer-controlled electromechanical universal testing machine (ETM 503B) with a shear rate of 2 mm/min, are used to evaluate the mechanical properties of Cu–Cu joints. For each case, eight samples are tested and the means and variances are calculated. To ensure the oxidation and reduction of Cu paste, the sintered Cu layers are analyzed by X-ray diffraction (XRD; PANalytical X'Pert Powder). The shear strengths are shown in Fig. 3(a). The chips almost detach from the DBC substrates (nearly 0 MPa) when the sintering atmosphere is pure argon. This is because that the Cu oxide is retained in the sintered-Cu when sintered in Ar environment and the Cu NPs cannot sintered. The copper oxide can be detected by XRD, and the results are shown in Fig. 3(b). When introduced with 5, 10, and 15 vol% of H_2, the corresponding bonding strength value are 4.13, 6.24, and 8.67 MPa, respectively. The bonding strength increased obviously with the increase of H_2 content. When further increasing the H_2 quantity of flow from 30 to 85 vol%, the bonding strength raised from 10.57 to 23.83 MPa. The strongest joints about 24.31 MPa are obtained at the point of 100 vol% H_2. The results indicate that the H_2 is helpful to improve the sintering qualities of the Cu–Cu joints due to the thermoreducibility of H_2. However, it can be founded from Fig. 3(a) that the strengthen effects decrease with the increase of H_2 addition, which means that the 85 vol% H_2 is enough to reduce the Cu oxide of paste. The reductive function can be confirmed by the XRD result, which is shown in Fig. 3(b). The complete XRD pattern of the paste is shown in Fig. S4. Diffraction peaks of Cu_2O and CuO are appeared in the unsintered Cu paste and the Cu layer sintered in Ar, while no copper oxide was detected in the Cu films sintered in 85% H_2 and 15% Ar. These findings indicate that the copper oxide can be completely removed by sintering in 85% H_2 and 15% Ar. In order to ensure the safety and take the sintering qualities of the joints into account, a sintering atmosphere of 85% H_2+15% Ar is determined for the sintering process.

III. Results and Discussion

A. Mechanical Characteristics

The shear strengths are used to illustrate the mechanical properties of large-area Cu–Cu joints. The shear strengths of

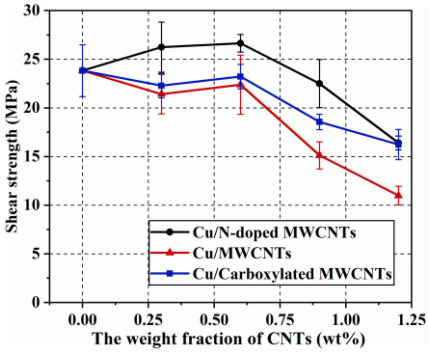

Fig. 4. Average shear strength of Cu–Cu joints bonded by Cu/CNTs composite paste against different CNTs weight fraction (0.0 wt% means pure Cu paste).

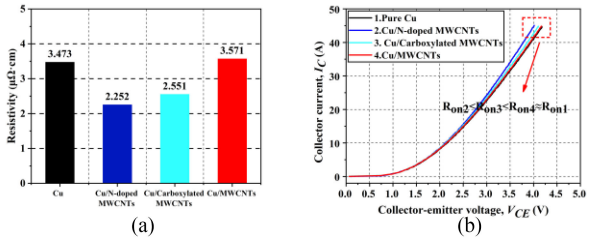

Fig. 5. Electrical properties. (a) Resistivity of bonding layers. (b) Static output characteristics of 3300 V/50 A IGBT modules.

the joints bonded Cu paste and three kinds Cu/CNTs composite paste are shown in Fig. 4. Introducing N-doped MWCNTs into Cu paste is able to enhance the joints bonding strength when the mass ratio below 0.6 wt%, whereas appears the opposite effect when the fraction exceeds 0.6 wt%. When 0.6 wt% N-doped MWCNTs are mixed, the joints achieve the strongest shear strength of 26.64 MPa, which is higher than that of pure Cu paste (23.83 MPa) and the die shear standard (MIL-STD-883K, 7.8 MPa). When the content of N-doped MWCNTs increased to 0.9 and 1.2 wt%, the joints' strength decreased to 22.5 and 16.4 MPa, respectively, which are lower than the pure Cu paste. Previous study reported that high shear strength (over 40 MPa) joints are obtained by sintered Cu [37], [38]. However, those successful bandings of robust joints have so far only reported for small area joints (<16 mm^2). It is difficult to realize high strength for the large-area die attach. The addition of MWCNTs and carboxylated MWCNTs damages the shear strength overall, especially when the percentage more than 0.6 wt%, the joints strengths decrease sharply. Compare with Cu/MWCNTs bonded joints, the Cu/carboxylated MWCNTs joints always shows better mechanical properties. This is due to that the oxygen-bearing of carboxylated MWCNTs improve the affinity of CNTs and Cu matrix [33]. However, the increase of affinity is not enough to make up for the negative effect of carboxylated MWCNTs on the joint shear strength. It will be discussed in detail later. On the whole, the variation trends of the joint strength with the increase of the addition amount of three kinds CNTs are similar, which do not change monotonously. In detail, when the percentage of CNTs increases from 0.3 to 0.6 wt%, the strength of the joint increases slightly, but decreases sharply when the CNTs weight fraction exceeds 0.6 wt%. These phenomena can be attributed to the influence of CNTs on the cracks and voids of the sintered layer, and we will analyze in detail later. According to the results, a percentage of 0.6 wt% for CNTs is considered as an optimal weight fraction in the Cu/CNTs, which can spur the bonding layer reach the best state and the percentage of 0.6 wt% is used in the following study.

B. Electrical Properties

The electrical properties are evaluated by the resistivity of the bonding layers and the static output *I–V* characteristics of the 3300 V/50 A IGBT modules, which are tested by four probe methods with a resistivity measurement system (AT510) and Agilent B1505A power device analyzer curve tracer, respectively. The specific preparation process of samples for resistivity tests and the test details are presented in the Supplementary Materials. In addition, the *I–V* curves setup image is shown in Fig. S3 in Supplementary Materials. As shown in Fig. 5(a), the resistivity of the sintered pure Cu layer is 3.473 $\mu\Omega$·cm, which is attributed to the high packing density of sintered Cu layer. When mixed with N-doped MWCNTs, the sintered composite film achieves the minimum resistivity of 2.252 $\mu\Omega$·cm, as low as 1.5 times of the bulk copper layer (1.68 $\mu\Omega$·cm), which, to the best of our knowledge, is the lowest resistivity using Cu paste for electrical packaging. The resistivities of Cu/carboxylated MWCNTs and Cu/MWCNTs are 2.551 and 3.571 $\mu\Omega$·cm, respectively. The results indicate that mixing functionalized MWCNTs with Cu paste increase electrical conductivity of the sintered layer. This is due to that mixing functionalized CNTs is able to reduce the porosities of bonding layer. In addition, the CNTs provide more electron transport channels and for conductive networks. [30], [39]. The poor adhesive strength of MWCNTs and Cu particles, caused more pores in the sintered layer. Thus, a higher resistivity is detected compared with that of the sintered pure Cu. The static output *I–V* curves of the demo devices are used to further confirm the positive effects of functionalized CNTs and the advantage of sintered Cu bonding technique. Due to the power limitation of the test equipment, our tests stopped when the collector current (I_C) reached 45 A. As presented in Fig. 5(b), the slope of the output *I–V* curves of the Cu/N-doped MWCNTs bonded devices is the largest, and that of Cu/carboxylated MWCNTs is follow, indicating that the electrical conductivities of the sintered Cu/functionalized CNTs layers are higher than the pure Cu. The curves of pure Cu and Cu/MWCNTs bonded devices are almost overlapped. This may be slightly affected by bonding lines or other factors. The tested results of electrical properties show that the introduction of functionalized CNTs is helpful to improve the electrical properties of Cu–Cu joints and verify the feasibility of sintered Cu bonding technology.

C. Microstructure Performances

The surface morphology of the sintered layer is observed by optical microscope (Olympus BX 41, Olympus, Japan). Fig. 6(a)–(e) exhibits the surface optical microphotographs of the sintered-layers containing different weight fraction N-doped MWCNTs. Because the effects of the content of three kinds of CNTs on the joint qualities are similar, we only show the images

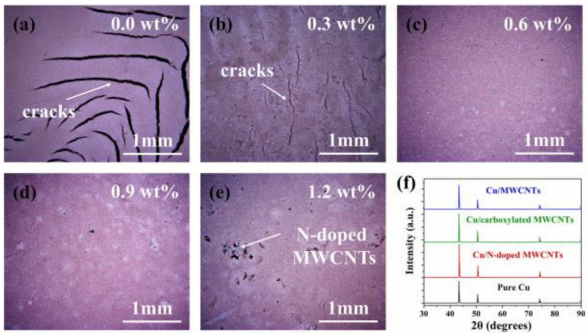

Fig. 6. (a)–(e) Surface optical microphotographs of sintered Cu/N-doped MWCNTs paste with different CNTs contents. (f) XRD pattern of four sintered paste films.

of sintered-Cu/N-doped MWCNTs layers Note that there are many cracks with different sizes in the central region of the sintered Cu layer, which are formed in the sintering process. Specifically, the organic solvents evaporate and produce capillary pressure, which need to be released by the pores. However, the organic vapor in the Cu–Cu joints with lager-area tend to be more difficult to be eliminated. Consequently, the pores developed into cracks and left in the sintered-layer, which will damage the sinterted qualities of bonding layer. By comparison, there are fewer cracks in the sintered-Cu/N-doped MWCNTs composite paste layer, as shown in Fig. 6(b)–(e). The reason could be that the organic vapor and stress can be released by the gaps between the CNTs and Cu particles, and the voids between the CNTs themselves. The gaps are caused by the poor affinity of CNTs and copper particles, which add the pores of the sintered layer. In addition, the CNTs cannot be connected to each other, thus, small holes appear around the CNTs. Besides, the holes increase with the growth of CNTs content. Hence, there are enough pores to relieve the stress and the discharge organic vapor, and the cracks in the sintered layer are avoided. Both the pores and the cracks in the bonding layer raise the porosities and further impair the qualities of the Cu–Cu joints. Therefore, only when the reduction of porosities due to the elimination of cracks is greater than that increased because of the added pores, the addition of CNTs can improve the density of the sintered layer and the qualities of the Cu–Cu joints. When 0.3 wt% CNTs were added, the cracks of the sintered layers are not completely eliminated, but pores have been added [seen in Fig. 6(b)]. Hence, the overall porosities increased. Only when the addition of CNTs reached 0.6 wt%, the density of sintered layer is improved. As we further increase the content of CNTs, the significantly increased porosity and the disjointed nature of the nanotubes resulted in a rapid deterioration in joint strength. This explains that why the joint strength does not change monotonously with the addition of CNTs. As the above analysis, when the addition is 0.6 wt%, the performance of the sintered layer is the best. Fig. 6(f) is the XRD pattern of sintered-Cu paste and three composite pastes with 0.6 wt% CNTs. No obvious Cu oxide phase peaks is detected by XRD, which indicates that the oxide of four pastes is sufficiently reduced in the atmosphere of 85% H_2+15% Ar. The addition of two functionalized MWCNTs has a positive effect on the sintered qualities. These results corresponded to that got from Figs. 4 and 5.

To investigate the bonding mechanisms of the large-area Cu–Cu joints, we observed the interface of the sintered layers and the fracture surface (internal structure) of joints by scanning electron microscope (SEM; Quattro S). As shown in Fig. 7(a), the pure Cu paste layer has been sintered into a thin film with a uniform porous structure. The nanosize particles melted and evolved into bonding necks and connected the adjacent microparticles. Fig. 7(e) is the fracture surface and Fig. 7(i) is the corresponding partial enlarge view. Obvious fracture traces and enlarged dimples that caused by ductile fracture are found in Fig. 7(e) and (i). However, some different sintering phenomena appear in the internal area of sintered film. The Cu particles are not uniformly sintered and part sintered-Cu phase seem denser and more compact, as shown in the yellow circle in Fig. 7(f). The condense phases are helpful for joint strength. From Fig. 7(j), the high magnification image of fracture surface, we learn that the Cu NPs adhere on the CNTs and keep their original shape. It is because that their sintering processes are disturbed by agglomerated CNTs. Fortunately, the aggregation degree of CNTs is light, and some fracture traces appear at the interface of sintered Cu near the CNTs, means that effective sintered necks are formed. Moreover, The N-doped MWCNTs have good adhesion with Cu NPs, which will be further testified later. Thus, mixing an appropriate amount (0.6 wt%) of N-doped MWCNTs is able to improve the joint strength. For Cu/carboxylated MWCNTs [seen in Fig. 7(c), (g), and (k)], the Cu particles are forced to separate by the gathered CNTs and cause some gaps. The fracture surface of Cu/carboxylated MWCNTs exhibits similar features to Cu/N-doped MWCNTs [seen in Fig. 7(g)]. But the agglomeration of carboxylated MWCNTs is more serious, which is disadvantageous to the joint strength. Since that the CNTs can not only be connected with each other, but also disturb the sintering of Cu NPs particles. Therefore, the addition of carboxylated MWCNTs cannot enhance joints strength. Thanks to the oxygen group, 0.6wt% carboxylated MWCNTs hardly damage the joints strength. The Cu particles on the surface of sintered Cu/MWCNTs film connect with adjacent particles and show a compact structure [seen in Fig. 7(d)]. But the MWCNTs cut off the connection between the condensed phase and the internal sintered Cu. More similar phenomena can be found in Fig. S6. In addition, some gaps between the Cu and MWCNTs can be found in Fig. 7(l) because of their poor bonding performance. The positive effect of the dense phase, marked by yellow circle in Fig. 7(h), cannot make up the damage of the MWCNTs cluster. Thus, the addition of MWCNTs simply damages the joint strength.

To further testify the adhesive strength of Cu and functionalized MWCNTs is stronger than that of Cu and MWCNTs and understand how the Cu NPs stick on the wall of CNTs, we observe the bonding condition of Cu and CNTs by transmission electron microscopy (TEM; FEI Talos F200S G2). The prepare process of TEM samples is described in the Supplementary Materials. Fig. 8(a)–(c) show the images of Cu/N-doped MWCNTs, and Fig. 8(j)–(m) are the mapping results of Fig. 8(c). It can be found that Cu NPs are adhered on the N-doped MWCNTs, while the microparticles and submicroparticls are removed by sonication.

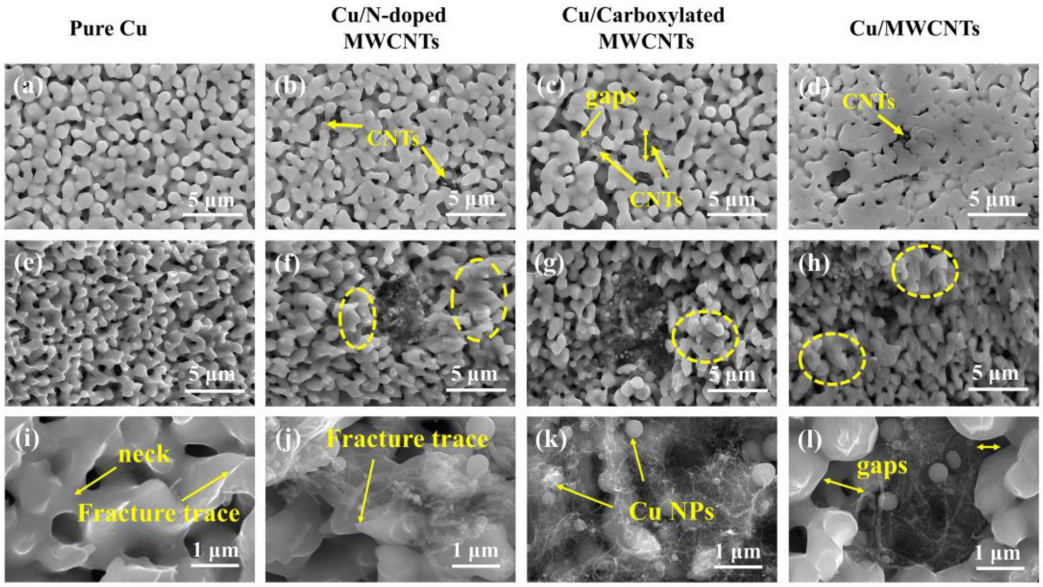

Fig. 7. (a)–(d) SEM images of sintered layers, (e)–(h) fracture microstructure of Cu–Cu joints, and (i)–(l) partial enlarged images of (e)–(h).

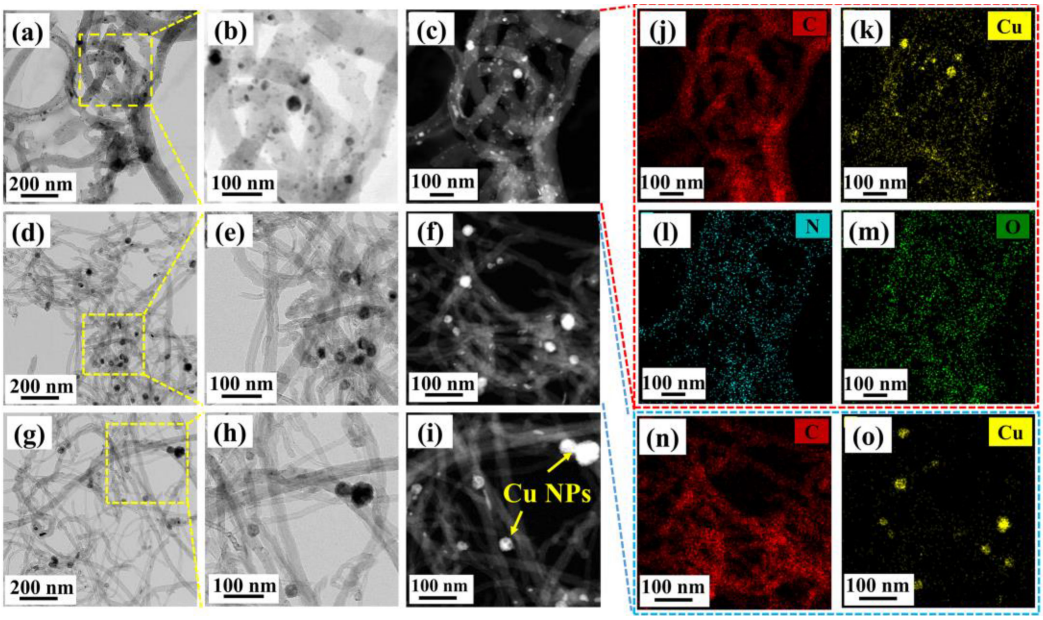

Fig. 8. TEM images of the interfacial bonding of Cu and CNTs. (a)–(c) Cu/N-doped MWCNTs, (d)–(f) Cu/Carboxylated MWCNTs and (g)–(i) Cu/MWCNTs. (j)–(m) are the mapping results of (c). (n)–(o) Corresponding elemental maps of (f).

This may be because the specific surface energy of Cu NPs is larger than that of micron and submicron Cu particles, and the nanoscale copper is easier to adhere to CNTs. As the mapping images shown, oxygen is detected in the composites, which could be due to the oxidation of copper in the sample preparation process and the residual organic solvents. Fig. 8(d)–(f) and Fig. 8(g)–(i) are the images of Cu/carboxylated MWCNTs and Cu/MWCNTs, and the Fig. 8(n)–(o) are the mapping results of Fig. 8(f). By comparing Fig. 8(b), (e), and (h), it can be found that the number of Cu NPs attached to the carboxylated MWCNTs is obviously less than that of N-doped MWCNTs, but it is more than that of MWCNTs. There are dense Cu NPs sticking to the wall of N-doped MWCNTs, but not so much on the carboxylated MWCNTs and MWCNTs. The elemental maps of Cu, Fig. 8(l) and (o), can also verify that the amounts of Cu NPs that are attached to the wall of N-doped MWCNTs are more than that of carboxylated MWCNTs. Previous studies have reported that the pyridine nitrogen atoms provide initial nucleation sites for the Cu nanoparticles and the strong nitrogen-metal bonding [40], [41]. The mixing of carboxylated MWCNTs can enhance the adhesive strength of Cu and CNTs since that the covalent functionalization improves the combination of interface strength [34]. Few Cu NPs cover on the MWCNTs since the inert nature of CNTs and the poor affinity with Cu. These observing results

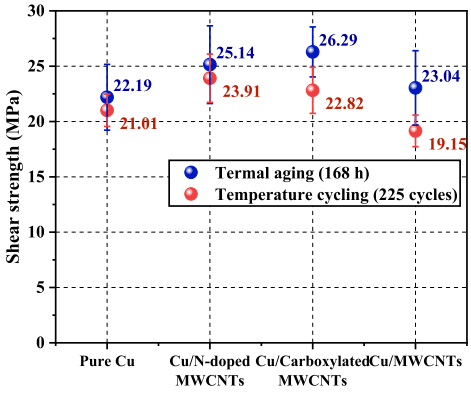

Fig. 9. Shear strength of the joints after thermal aging and temperature cycling.

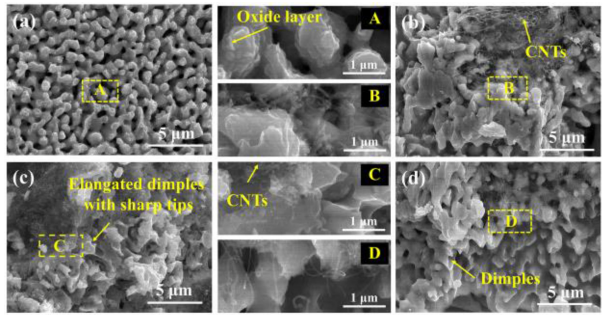

Fig. 10. Fracture surfaces. (a) Pure Cu bonded joints, (b) Cu/N-dopedd MWCNTs bonded joints, (c) Cu/carboxylated MWCNTs bonded joints, and (d) Cu/MWCNTs bonded joints. The middle four small pictures correspond to the local enlarge images of A, B, C, and D in (a), (b), (c), and (d), respectively.

agree well with the shear strength and the fracture images results. According the above comparison, it can draw a conclusion that the functionalization can improve the adhesion of Cu and CNTs, and the enhancement effect of N-doped MWCNTs is the strongest. So, the functionalization is an effective route to improve the Cu/CNTs binding energies.

D. Reliability Test

The reliability of the Cu–Cu joints was assessed by both thermal aging tests and temperature cycling tests. The thermal aging was conducted at 250 °C in air for 168 h and the joint's shear strength was tested. The temperature cycling tests were carried out in a thermal shock chamber (ATEC, CST200S) from -65 to 150 °C, and 225 cycles were subjected. Each cycle lasts about 54 min, which includes a constant dwell time of 12 min (The MIL-STD-883K suggests the dwell time for at least 10 min) at both maximum and minimum temperature and 15 min at both heating and cooling stages. The joints' strength after thermal aging and temperature cycling tests are shown in Fig. 9. Before thermal aging, the bonding strength of the pure Cu bonded joints is 23.83 MPa (seen in Fig. 4). The joints strength decreased to 22.19 MPa after thermal aging, only 6.88% lower than the fresh joints. The joints strength achieved by Usui *et al.* [22] decreased greatly after thermal aging in 250 °C for 100 h. This indicates that the sintered Cu bonding technology possesses better long-term reliability than previous studies. As for the Cu/N-doped MWCNTs bonded joints, the strength decreases from 26.64 to 25.14 MPa, drops only 5.74%, which shows a better long-term reliability than pure Cu. We are surprised to find that the shear strength of Cu/carboxylated MWCNTs and Cu/MWCNTs bonded joints do not decreases but increases after thermal aging. As shown in the Fig. 9, the strengths are increased from 23.22 to 26.29 MPa for Cu/carboxylated and from 22.38 to 23.04 MPa for Cu/MWCNTs. The reason could be that the sintered layer is so dense that little oxygen can flow into the internal, and the oxidation degree of the bonding layer is very low. In addition, the bondlines may further experience the processes of densification and grain growth.

The shear strengths of the four types joints after temperature cycling treatments drop obviously, and the values for pure Cu, Cu/N-doped MWCNTs, Cu/carboxylated MWCNTs, and Cu/MWCNTs are 88.17%, 89.75%, 98.32%, and 85.57% of the initial values, respectively (for more details, see Supplementary Material). The decrease degrees of pure Cu and Cu/MWCNTs bonded joints are clearly higher than that of the Cu/functionalized MWCNTs bonded joints. The Cu/N-doped MWCNTs joints exhibit higher strength (23.91 MPa) than that of the fresh pure Cu joints (23.83 MPa), even after 225 thermal cycles. As for the Cu/caboxylated MWCNTs joints, the strength drops only 1.68% (from 23.22 to 23.82 MPa), and achieves comparable value with the fresh pure Cu joints. The reduction of the joint's strength is due to that the sintered layers experience complex microstructure degradation driven by temperature cycling, involving the oxidation of material, crack initiation, and fatigue propagation of the already existing defects. The lower deterioration degree of Cu/functionalized MWCNTs bonded joints could be attributed that the functionalized MWCNTs cannot only eliminate the sintered Cu layer cracks and decrease the initial defects of Cu–Cu joints, but also improve the durability of the sintered layers. The internal evolution of the bonding layer after reliability tests is analyzed by observing the fracture surface.

The fracture surfaces of the joints after thermal aging are shown in Fig. 10. The developments of Cu particles in four type joints are various. For the joint bonded by pure Cu paste, as shown in Fig. 10(a), the sintered necks that act as bridges connecting the Cu microparticles further coarsened, indicating a higher sintering level. The broadened sintered necks enhance the joints strength. However, the fracture traces, and dimple structure caused by ductile fracture are not so obvious in pure Cu joints. In addition, the sintered Cu is obviously oxidized and the surface morphology has changed greatly. Oxide shell with sarcomatous-like shape grows on the smooth surface, and the oxide shell has a tendency of peeling. The fracture of sintered layer is composed of brittle fracture of copper oxide shell and ductile fracture of pure copper core. Therefore, the trace of ductile fracture trace weakens and joints strength decreases. It can be inferred that when oxygen intrudes into the copper, the fracture mode of the joint will be completely converted into brittle fracture, at which time the strength of the joint will drop sharply. For the joints bonded by Cu and CNTs composite paste, it can be found that obvious densification occurred in the

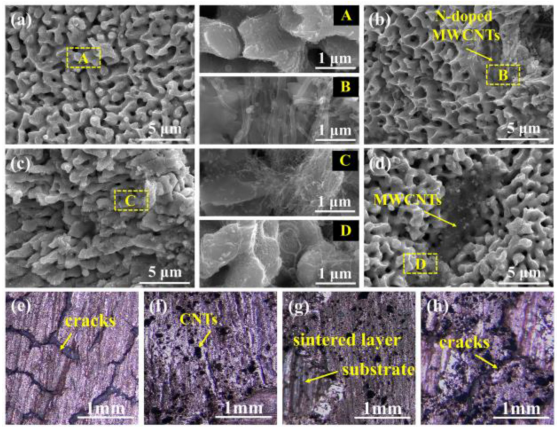

Fig. 11. SEM images and optical microphotographs of fracture surfaces. (a) and (e) Pure Cu bonded joints, (b) and (f) Cu/N-dopedd MWCNTs bonded joints, (c) and (g) Cu/carboxylated MWCNTs bonded joints, and (d) and (h) Cu/MWCNTs bonded joints. The middle four small pictures correspond to the local enlarge images of A, B, C, and D in (a), (b), (c), and (d), respectively.

bonding layers [Fig. 10(b) and (c)], which induces the emergence of dense phase with nonspherical and irregular shape. There is few Cu NPs adhere to the CNTs, especially in fracture surfaces of Cu/carboxylation MWCNTs and Cu/MWCNTs, which is responsible for the secondary sintering of Cu NPs during the thermal aging. In contrast, the secondary sintering degree of Cu NPs in N-doped MWCNTs may be the weakest, because there are spherical Cu NPs remain in the Fig. 10(b). In the local enlarged image of Fig. 10(b), some signs of copper oxide growth on the sintered Cu surface are found. These performances may be the reason for the decrease of shear strength of N-doped MWCNTS bonded joints. Fig. 10(c) and (d) exhibit typical morphology of ductile fracture joints that possess many elongated dimples with sharp tips, indicating that the joints still have reliable interconnections. The dimples are enlarged in the middle little pictures. The observing results indicate that the sintered Cu/functionalized MWCNTs layers are highly stable against thermal aging, which are in good agreement with the shear strength that shown in Fig. 9. The contained effects of compact bonding layer on the oxidation of sintered Cu and the further densification process of sintered Cu work together in against the thermal aging.

It has been reported by the previous studies that the thermal mismatches among Si chips, sintered-layers, and DBC substrates can generate thermomechanical stress during temperature cycling, which will worsen the shear strength of the samples [42], [43]. Fig. 11 shows the fracture surfaces of the joints after temperature cycling. The microscopic structure cannot present the thermo-mechanical stress caused by temperature changes, but it can reveal the current interconnected behaviors and the deterioration degree of the bonding layers. As presented in Fig. 11(a)–(d), each kind of joint's fracture surfaces exhibits traces of ductile fracture and the most obvious is that bonded by Cu/N-doped MWCNTs. As mentioned early, the elongated and sharp dimples indicate the high shear strength of the Cu–Cu joint. In addition, it can be found that the sintered Cu has been further coarsened and almost lost the original shape. Such coarsening mechanism promotes the joints more difficult to break. Therefore, the joints possess high reliability. However, it can be seen from the local enlarged views of A, B, C, and D that the sintered Cu is oxidized. This is one of the reasons that the joint's strength is detected to be deteriorated. The other main reason is that the cracks and other initial defects developed in the bonding layer during the temperature cycling, as shown in Fig. 11(e)–(h). The debonding mode of the four types Cu–Cu joints is surface failure, and the break sites are mainly on the back of the upper chips. Fig. 11(e) is the surface optical microphotographs of sintered pure Cu. Many cracks are found on the fracture surface of the sintered pure Cu layer, which are caused by the thermal stress in the bonding layer. Cracks are also detected on the broken sintered Cu/MWCNTs joints. While the fracture surfaces of the sintered Cu/functionalized layers show few cracks, but only some bumps and holes appear on the interface. These phenomena indicate that the sintered Cu/functionalized joints are only slightly damaged after 225 temperature cycles. Thus, the joints present higher shear strength than the pure Cu joints and Cu/MWCNTs joints.

IV. Conclusion

In this article, we investigated the optimal presintering temperature and sintering atmosphere for die attachment. High strength (23.83 MPa) and high reliable Cu–Cu joints are obtained by sintering multiscale Cu paste in 85% H_2+15% Ar with a persintering temperature of 160 °C. More importantly, we found that the joints qualities are effectively improved by introducing 0.6 wt% functioned MWCNTs into Cu paste. Specifically, the introduction of N-doped MWCNTs plays a positive effect on joint strength. One reason is that the addition of moderate CNTs is able to avoid cracks and decrease the porosities of the bondline. The other reason is that the presence of functional groups can improve the adhesive strength of Cu and CNTs. The electrical resistivities of the sintered layer decrease from 3.473 to 2.252 $\mu\Omega$·cm when mixing with N-doped MWCNTs and to 2.551 $\mu\Omega$·cm when adding carboxylated MWCNTs. The improvement in conductivity is attributed not only to the higher density of the sintered layer, but also to the role of carbon nanotubes as electron channels in the bonding line. Both the addition of N-doped MWCNTs and carboxylated MWCNTs work on improving the reliability of the joints, which can be attribute to the compact bonding layer and the further sintering behavior of Cu NPs. Thus, Cu/functionalized MWCNTs composite paste shows great potential for using in building high performance die attachment. And the finding of this article is helpful for WBG power electrics packaging.

References

[1] J. Hornberger, A. B. Lostetter, K. J. Olejniczak, T. McNutt, S. M. Lal, and A. Mantooth, "Silicon-carbide (SiC) semiconductor power electronics for extreme high-temperature environments," *IEEE Aerosp. Conf. Proc.*, vol. 4, no. 12, pp. 2538–2555, Mar. 2004.

[2] T. Nomura, M. Masuda, N. Ikeda, and S. Yoshida, "Switching characteristics of ganhfets in a half bridge package for high temperature applications," *IEEE. Trans. Power Electr.*, vol. 23, no. 2, pp. 692–697, Mar. 2008.

[3] J. Rabkowski, D. Peftitsis, and H. Nee, "Silicon carbide power transistors: A new era in power electronics is initiated," *IEEE Ind. Electron. Mag.*, vol. 6, no. 2, pp. 17–26, Jun. 2012.
[4] J. Millan, P. Godignon, X. Perpina, A. Perez-Tomas, and J. Rebollo, "A survey of wide bandgap power semiconductor devices," *IEEE Trans. Power Electron.*, vol. 29, no. 5, pp. 2155–2163, May 2014.
[5] R. Khazaka, L. Mendizabal, D. Henry, and R. Hanna, "Survey of high-temperature reliability of power electronics packaging components," *IEEE. Trans. Power Electr.*, vol. 30, no. 5, pp. 2456–2464, May 2015.
[6] H. S. Chin, K. Y. Cheong, and A. B. Ismail, "A review on die attach materials for sic-based high-temperature power devices," *Metal. Mater. Trans. B*, vol. 41, no. 4, pp. 824–832, Aug. 2010.
[7] S. W. Yoon, M. D. Glover, and K. Shiozaki, "Nickel–Tin transient liquid phase bonding toward high-temperature operational power electronics in electrified vehicles," *IEEE Trans. Power Electron.*, vol. 28, no. 5, pp. 2448–2456, May 2013.
[8] M. Wang, Y. Mei, X. Li, R. Burgos, D. Boroyevich, and G.-Q. Lu, "Pressureless silver sintering on nickel for power module packaging," *IEEE Trans. Power Electron.*, vol. 34, no. 8, pp. 7121–7125, Aug. 2019.
[9] M. Li, Y. Xiao, Z. Zhang, and J. Yu, "Bimodal sintered silver nanoparticle paste with ultrahigh thermal conductivity and shear strength for high temperature thermal interface material applications," *ACS Appl. Mater. Interf.*, vol. 7, no. 17, pp. 9157–9168, May 2015.
[10] S. Gao *et al.*, "Bonding of large substrates by silver sintering and characterization of the interface thermal resistance," *IEEE. Trans. Ind. Appl.*, vol. 55, no. 2, pp. 1828–1834, Mar./Apr. 2019.
[11] J. W. Yoon and J. H. Back, "Effect of sintering conditions on the mechanical strength of Cu-sintered joints for high-power applications," *Mater. (Basel)*, vol. 11, no. 11, Oct. 2018, Art. no. 2105.
[12] R. Watanabe and T. Ishizaki, "Enhancement of pressure-free bonding with Cu particles by the addition of Cu–Ni alloy nanoparticles," *J. Mater. Chem. C*, vol. 2, no. 18, pp. 3542–3548, 2014.
[13] R. Riva, C. Buttay, B. Allard, and P. Bevilacqua, "Migration issues in sintered-silver die attaches operating at high temperature," *Microelectron. Reliab.*, vol. 53, nos. 9-11, pp. 1592–1596, Sep.–Nov. 2013.
[14] J. Liu, H. Chen, H. Ji, and M. Li, "Highly conductive cu-cu joint formation by low-temperature sintering of formic acid-treated cu nanoparticles," *ACS Appl. Mater. Interf.*, vol. 8, no. 48, pp. 33289–33298, Dec. 2016.
[15] Y. Zuo, J. Shen, J. Xie, and L. Xiang, "Influence of Cu micro/nano-particles mixture and surface roughness on the shear strength of Cu-Cu joints," *J. Mater. Process. Technol.*, vol. 257, pp. 250–256, 2018.
[16] O. V. Dement'eva and V. M. Rudoy, "Copper nanoparticles synthesized by the polyol method and their oxidation in polar dispersion media. The influence of chloride and acetate ions," *Colloid J*, vol. 74, no. 6, pp. 668–674, Nov. 2012.
[17] M. Bicer and I. Sisman, "Controlled synthesis of copper nano/microstructures using ascorbic acid in aqueous CTAB solution," *Powder Technol*, vol. 198, no. 2, pp. 279–284, Mar. 2010.
[18] Y. Gao *et al.*, "Die bonding performance using bimodal cu particle paste under different sintering atmospheres," *J. Electron. Mater.*, vol. 46, no. 7, pp. 4575–4581, 2017.
[19] I. Kim and J. Kim, "The effect of reduction atmospheres on the sintering behaviors of inkjet-printed Cu interconnectors," *J. Appl. Phys.*, vol. 108, no. 10, Nov. 2010, Art. no. 102807.
[20] K. Woo, Y. Kim, B. Lee, J. Kim, and J. Moon, "Effect of carboxylic acid on sintering of inkjet-printed copper nanoparticulate films," *ACS Appl. Mater. Interfaces*, vol. 3, no. 7, pp. 2377–2382, Jul. 2011.
[21] Y. Tian *et al.*, "Sintering mechanism of the Cu-Ag core-shell nanoparticle paste at low temperature in ambient air," *RSC Adv*, vol. 6, no. 94, pp. 91783–91790, 2016.
[22] M. Usui *et al.*, "Effects of thermal aging on Cu nanoparticle/Bi-Sn solder hybrid bonding," *Microelectron. Reliab.*, vol. 78, pp. 93–99, 2017.
[23] Y. Y. Dai *et al.*, "Enhanced copper micro/nano-particle mixed paste sintered at low temperature for 3D interconnects," *Appl. Phys. Lett.*, vol. 108, no. 26, 2016, Art. no. 263103.
[24] T. Ishizaki *et al.*, "Reliability of Cu nanoparticle joint for high temperature power electronics," *Microelectron. Reliab.*, vol. 54, no. 9–10, pp. 1867–1871, 2014.
[25] T. Ishizaki *et al.*, "Power cycle reliability of Cu nanoparticle joints with mismatched coefficients of thermal expansion," *Microelectron. Reliab.*, vol. 64, pp. 287–293, 2016.
[26] S. Zhang *et al.*, "Carbon-nanotube-based electrical conductors: Fabrication, optimization, and applications," *Adv. Electro. Mater.*, vol. 5, no. 6, Jun. 2019, Art. no. 1800811.
[27] P. Dariyal, A. K. Arya, B. P. Singh, and S. R. Dhakate, "A review on conducting carbon nanotube fibers spun via direct spinning technique," *J. Mater. Sci.*, vol. 56, no. 2, pp. 1087–1115, 2020.
[28] S. Zhang, J. G. Park, N. Nguyen, C. Jolowsky, A. Hao, and R. Liang, "Ultra-high conductivity and metallic conduction mechanism of scale-up continuous carbon nanotube sheets by mechanical stretching and stable chemical doping," *Carbon*, vol. 125, pp. 649–658, 2017.
[29] F. Daneshvar, T. Zhang, A. Aziz, H. J. Sue, and M. E. Welland, "Tuning the composition and morphology of carbon nanotube-copper interface," *Carbon*, vol. 157, pp. 583–593, Feb. 2020.
[30] H.-J. Hwang, S.-J. Joo, and H.-S. Kim, "Copper nanoparticle/multiwalled carbon nanotube composite films with high electrical conductivity and fatigue resistance fabricated via flash light sintering," *ACS Appl. Mater. Interfaces*, vol. 7, no. 45, pp. 25413–25423, Nov. 2015.
[31] C. Bittencourt *et al.*, "Study of the interaction between copper and carbon nanotubes," *Chem. Phys. Lett.*, vol. 535, pp. 80–83, 2012.
[32] P.-M. Hannula *et al.*, "Observations of copper deposition on functionalized carbon nanotube films," *Electrochim. Acta*, vol. 232, pp. 495–504, 2017.
[33] K. Z. Milowska, M. Burda, L. Wolanicka, P. D. Bristowe, and K. K. K. Koziol, "Carbon nanotube functionalization as a route to enhancing the electrical and mechanical properties of Cu-CNT composites," *Nanoscale*, vol. 11, no. 1, pp. 145–157, Dec. 2018.
[34] M. Park, B.-H. Kim, S. Kim, D.-S. Han, G. Kim, and K.-R. Lee, "Improved binding between copper and carbon nanotubes in a composite using oxygen-containing functional groups," *Carbon*, vol. 49, no. 3, pp. 811–818, 2011.
[35] K. T. Kim, S. I. Cha, T. Gemming, J. Eckert, and S. H. Hong, "The role of interfacial oxygen atoms in the enhanced mechanical properties of carbon-nanotube-reinforced metal matrix nanocomposites," *Small*, vol. 4, no. 11, pp. 1936–1940, Nov. 2008.
[36] Y. Morisada *et al.*, "A low-temperature pressureless bonding process using a trimodal mixture system of Ag nanoparticles," *J. Electron. Mater.*, vol. 40, no. 12, pp. 2398–2402, 2011.
[37] J. Liu, H. Chen, H. Ji, and M. Li, "Highly conductive cu-cu joint formation by low-temperature sintering of formic acid-treated Cu nanoparticles," *ACS Appl. Mater. Interf.*, vol. 8, no. 48, pp. 33289–33298, Dec. 2016.
[38] Y. Peng, Y. Mou, J. Liu, and M. Chen, "Fabrication of high-strength Cu–Cu joint by low-temperature sintering micron–nano Cu composite paste," *J. Mater. Sci. Mater. Electron.*, vol. 31, no. 11, pp. 8456–8463, 2020.
[39] S. Fu, X. Chen, and P. Liu, "Preparation of CNTs/Cu composites with good electrical conductivity and excellent mechanical properties," *Mater. Sci. Eng. A-Struct.*, vol. 771, 2020, Art. no. 138656.
[40] V. G. Ramu, A. Bordoloi, T. C. Nagaiah, W. Schuhmann, M. Muhler, and C. Cabrele, "Copper nanoparticles stabilized on nitrogen-doped carbon nanotubes as efficient and recyclable catalysts for alkyne/aldehyde/cyclic amine A(3)-type coupling reactions," *Appl. Catal. A-Gen.*, vol. 431, pp. 88–94, Jul. 2012.
[41] K. Z. Milowska, M. Burda, L. Wolanicka, P. D. Bristowe, and K. K. K. Koziol, "Carbon nanotube functionalization as a route to enhancing the electrical and mechanical properties of Cu- CNT composites," *Nanoscale*, vol. 11, no. 1, pp. 145–157, Jan. 2019.
[42] K.-C. Wu, S.-Y. Lin, T.-Y. Hung, and K.-N. Chiang, "Reliability assessment of packaging solder joints under different thermal cycle loading rates," *IEEE Trans. Device Mater. Rel.*, vol. 15, no. 3, pp. 437–442, Sep. 2015.
[43] T. F. Chen and K. S. Siow, "Comparing the mechanical and thermal-electrical properties of sintered copper (Cu) and sintered silver (Ag) joints," *J. Alloy Compd.*, vol. 866, 2021, Art. no. 158783.

Lingmei Wu received the B.S. degree from Shandong University of Science and Technology, Shandong, China, in 2018.

She is currently the Graduate Student with Electrical Engineering College and State Key Laboratory of Power Transmission Equipment and System Security and New Technology, Chongqing University, Chongqing, China. Her current research interests include power electronic packaging and die-attachmen materials.

Jing Qian received the B.S. degree in mechanical design manufacture and automation major from Jinling Institute of Technology, Nanjing, China, in 2017, and the M.Sc. degree in mechanical engineering from Guilin University of Electronic Technology, Guilin, China, in 2020.

His current research interests include the packaging of power electronics.

Fusheng Zhang received the B.S. degree from Chongqing Jiaotong University, Chongqing, China, in 2019.

He is currently the Graduate Student with the Electrical Engineering College, Chongqing University, Chongqing, China.

His current research interests include computational materials design for energy and sensing applications including thermoelctric and gas sensors.

Jiabing Yu received the B.Sc. degree from the University of Science and Technology of China, Hefei, China, in 2013, and the Ph.D. degree majored in mechanics (advanced materials and mechanics) from Peking University, Beijing, China, in 2019.

He is currently with the School of Optoelectronic Engineering, Chongqing University, Chongqing, China. His current research interests include computational materials design for energy and sensing applications, including thermoelectric, gas sensors.

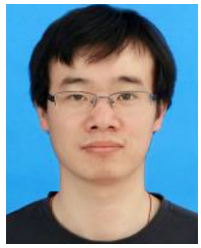

Ze-Ping Wang received the Ph.D. degree in engineering from Chongqing University, Chongqing, China, in 2021.

He is currently a Postdoctor with Fujian Institute of Research on the Structure of Matter, the Chinese Academy of Sciences, Beijing, China. His current research interests include smart materials and devices.

Haojie Guo received the B.E. degree from the North University of China, Taiyuan, China, in 2019.

He is currently the Graduate Student with Optoelectronic Engineering College, Chongqing University, Chongqing, China.

His current research interests include power electronics packaging, and gas sensors with high performance.

Xianping Chen (Senior Member, IEEE) received the B.Eng. degree from Chongqing University (CQU), Chongqing, China, in 2002, the M.Sc. degree from Dresden University of Technology, Dresden, Germany, in 2006, and the Ph.D. degree from Delft University of Technology, Delft, The Netherlands, in 2013.

He was Postdoctoral Researcher with Tsinghua University, Beijing, China, from 2013 to 2015. He is currently a Full-Time Professor with the School of Electrical Engineering and State Key Laboratory of Power Transmission Equipment and System Security and New Technology, Chongqing University, Chongqing, China. He is also the Distinguished Expert with Chongqing Municipality, China, and the Technical Committee Member of China Advanced Semiconductor Industry Innovation Alliance. He authored or coauthored about 80 technical papers (more than 50 SCI journal publications) and four books. He holds 41 patents. His research interests include electronic materials, electronic packaging, chemical and biological sensors, LED, and nanodevices.

Dr. Chen was a recipient of the One-Hundred Talent Program Scholars of Guangxi in 2013 and the One-Hundred Talent Program Scholars of Chongqing Municipality in 2016, respectively. (Based on document published on 9 August 2017).